Online Hypermodel-based Path Planning for Feedback Control of Tissue Denaturation in Electrosurgical Cutting

Hamza El-Kebir *, **Yongseok Lee** **, **Richard Berlin** ***,
Enrico Benedetti ****, **Pier C. Giulianotti** †,
Leonardo P. Chamorro ‡, **Joseph Bentsman** §

* *Department of Aerospace Engineering, University of Illinois, Urbana, IL 61801 USA (e-mail: elkebir2@illinois.edu)*
** *Department of Mechanical Science and Engineering, University of Illinois, Urbana, IL 61801 USA (e-mail: yl50@illinois.edu)*
*** *Trauma Surgery, Carle Hospital, Urbana, IL 61801 USA*
**** *Department of Surgery, UI Health, Chicago, IL 60612 USA*
† *Division of Minimally Invasive, General & Robotic Surgery, University of Illinois at Chicago, Chicago, IL 60612 USA*
‡ *Department of Mechanical Science and Engineering, University of Illinois, Urbana, IL 61801 USA*
§ *Department of Mechanical Science and Engineering, University of Illinois, Urbana, IL 61801 USA (e-mail: jbentsma@illinois.edu)*

Abstract: The first closed-loop control of electrosurgical power satisfying a specified tissue damage bound along the desired tissue dissection path is presented. The damage is represented by the $82\,^\circ$C isotherm corresponding to the admissible tissue denaturation front position in relation to that of the cutting probe tip. The front location is assessed in real time through the infrared temperature readings of the $40\,^\circ$C isotherm tightly related to the emerging denaturing patch size around the moving probe tip. A control-oriented denaturing hypermodel and its recasting into a form amenable for use in a moving-horizon locally linear model predictive control law are presented. The optimal control action is determined by solving a compound model predictive control problem that targets a number of active one-dimensional domains. This model is obtained from an offline trained nonlinear autoregressive model with exogenous input. To enforce the safety constraints, a supervisor system precedes the path planning control law. This system prevents excessive denaturation by excluding certain system moves, and determines system termination conditions. We experimentally demonstrate the system's performance in two different line-cutting tasks on ex vivo porcine tissue with a desired denaturation front.

Keywords: Medical robots and systems, autonomous robotic surgery, model-based planning.

1. INTRODUCTION

Over the past decades, the advantages of robot-assisted surgery over conventional laparoscopy have become increasingly apparent (Beasley, 2012). As the performance demands on the robotic surgery tools grow, so does the need for a deeper understanding of the physical phenomena that govern both the tools and the tissue treated, as well as the control laws for the precise attainment of the surgical objectives.

Electrosurgery relies on the use of high power density radio frequency currents to actively heat organic tissue, allowing it to be denatured, coagulated, desiccated, fulgurated, or

incised (Palanker et al., 2008). One of the key advantages of electrosurgery is its simultaneous cutting and coagulation capability, providing blood stoppage for complex surgical tasks. Since this technique allows for precise ablation of tissue with very little collateral damage (∼100–400 μm), it is commonly used in practice, with over half of the surgical procedures employing it (Palanker et al., 2008). One of the key disadvantages of human-operated electrosurgery is, however, the tendency to damage nearby tissue due to an excessive influx of heat (Palanker et al., 2008). The effects of this damage are not apparent to the surgeon during operation, and appear only hours to days after being inflicted. An illustration of the electrosurgical process is shown in Fig. 1.

Here, we present a novel closed-loop-conditioned path planning technique autonomously satisfying the specified electrosurgical tissue denaturation bound, with built-in measures to prevent tissue charring. Strict termination conditions based on the spatial maximum temperature
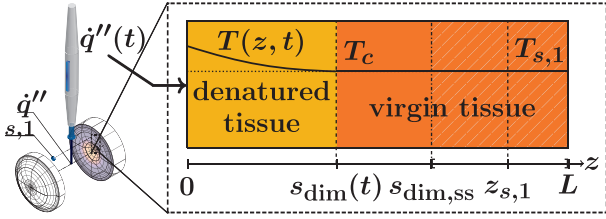
Fig. 1. Exploded view of laparoscopic electrosurgical operation, with the two semi-spheres designating the tissue. Here, $s_{\dim}$ denotes the phase-change interface (PCI) location, with $s_{\dim,\,ss}$ denoting its steady-state.
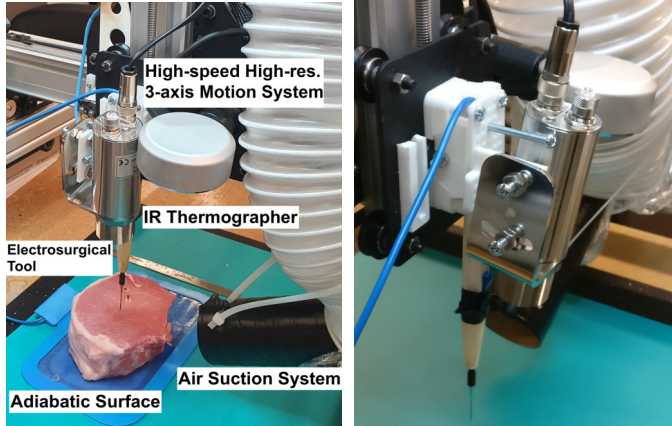

Fig. 2. Experimental setup illustrating the electrosurgical tool, three-axis motion system, and IR thermographer (left), and a closer view (right).

field are implemented to terminate the system before excessive damage is imparted onto the tissue. The explicit objective is to attain full control of the tissue denaturation front along the tissue dissection path. To the best of the authors' knowledge, the demonstrated path-planning/control law is the first temperature-feedback and model-based autonomous electrosurgical tool developed in the literature.

2. PRIOR WORK

The electrosurgical control problem can be posed as a boundary control problem characterized by a controllable heat flux, as dictated by the power setting, and cathode position actuation. Describing the dynamics of heat propagation in the tissue is a nontrivial problem; as the first approximation, we consider a homogeneous substance undergoing a moving phase change from *virgin* to *denatured* tissue. This allows casting the denaturation control problem as a *Stefan problem* (Cannon, 1984), in which the control object is the moving phase-change interface (PCI), and the manipulated variable (i.e., control input) is the heat flux.

We have previously developed a novel pointwise non-collocated feedback control law for the Stefan problem in (El-Kebir and Bentsman, 2021) for a stationary heat source. However, in electrosurgery the heat source is moving. Therefore, rather than controlling the PCI location on a 1-D domain, the present work aims at addressing the problem of path planning when operating on a 2-D tissue surface. Saeidi et al. (2019) considered a fixed power level and probe velocity in their path planning,
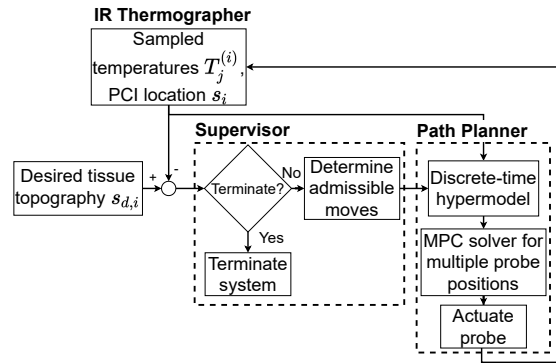

Fig. 3. Control logic of the hypermodel-based electro-surgery path planning method.

providing feedback only through trajectory deviation as obtained from infrared and visible light cameras. Using their approach, however, tissue damage is not factored into feedback, resulting in an appreciable amount of tissue charring. Opfermann et al. (2017) replaced the tissue and probe dynamics by heuristic observations of tissue charring, which allowed them to approximate the level of charring for a number of tissue types. Their approach relied on computer vision to account for path tracking error, but functioned in an open loop fashion with regards to the probe's power level and duty cycle. This implies that any spurious tissue reactions would not be accounted for, and significant tissue damage could be imparted if the system were to run fully autonomously.

In this work, we investigate the problem of path planning in the context of electrosurgical control, with the explicit goal of minimizing tissue damage. In particular, the main objective is to induce a desired denaturation front by *simultaneously controlling both the position and the power output* of the electrosurgical probe. To this end, we present a novel approach that leverages a spatial temperature field and incorporates a hypermodel that maps the state of a 1-D temperature domain to a discrete-time model of the phase-change interface dynamics subject to a boundary heat flux input. These models are then used to solve a moving-horizon model predictive control problem involving both the power input to the model from the probe and the probe location, providing a feedback-based path planning approach for controlling tissue denaturation. The loop is closed by feedback from an infrared (IR) thermographer. Basic features of the experimental setup are shown in Fig. 2.

The hypermodel considers step input responses of the tissue PCI given a temperature field, using a wavelet-based nonlinear system identification technique (Billings and Wei, 2005). Given this hypermodel, a compound model of several 1-D domains across the tissue can be generated. For each of the models, a constrained moving horizon model predictive control (MPC) problem is solved. Since the compound model that is obtained is linear, it is possible to regulate the phase-change interface tracking errors, thereby tracking the desired denaturation front. Based on the minimum cost attained the probe will either remain stationary or move while applying the electrosurgical action. A flowchart detailing this process is given in Fig. 3.

3. METHODS

We developed analytically and numerically, and implemented in hardware, a control system based on an electrosurgical power supply unit and a versatile, fully-customizable 3-axis gantry system, which is used to perform a number of line cutting tasks on ex vivo porcine tissue, while maintaining the desired denaturation front to limit heat damage to the tissue. The system is capable of running autonomously by virtue of local temperature field feedback from a compact infrared thermographer, an Optrix Xi 400 sensor with microscopic optics (Optris GmbH). The system is shown in Fig. 2.

We first present the formulation of our control-oriented one-dimensional tissue denaturation model, which will be used to obtain a nonlinear discrete-time model of the phase-change dynamics. The nonlinearity in the identified model is represented through wavelet regressors. This nonlinear model, which we call the *hypermodel*, is dependent on the current temperature field, allowing us to represent the local linear phase-change interface dynamics for one-dimensional slices in the problem domain. We present a means of obtaining the local linear dynamics, as well as a method of combining a number of one-dimensional domains into a compound linear model based on a heat flux distribution model.

Following this, we present the model predictive control (MPC) architecture that we will leverage to obtain our path. This architecture is comprised of a supervisor system that provides a set of admissible movements as well as system termination conditions, followed by a path planner, which solves the MPC problem for three probe locations, and executes the control policy that is optimal in a sense that will be defined later.

3.1 Control-oriented Hypermodel

In El-Kebir and Bentsman (2021), we have argued that the one-dimensional two-phase Stefan problem forms an adequate control-oriented model for the stationary electrosurgical impact. This model is based on a one-dimensional domain, with Fourier heat transfer across two phases representing, respectively, *virgin* and *denatured* tissue separated by a phase-change-interface (PCI), as shown in Fig. 1. This one-dimensional model will be leveraged to generate a hypermodel, as described in this section.

Two-phase One-dimensional Stefan Problem. We present here a non-dimensional formulation of the two-phase Stefan problem, based on an energy balance at the phase-change interface (El-Kebir and Bentsman, 2021): $\frac{\partial \theta(\xi,\tau)}{\partial \tau} = \frac{\partial^2 \theta(\xi,\tau)}{\partial \xi^2}$, for $\tau > 0$ and $\xi \in (0,1) \setminus \{s(\tau)\}$, subject to $-\left.\frac{\partial \theta(\xi,\tau)}{\partial \xi}\right|_{\xi=0} = u(\tau)$, $\left.\frac{\partial \theta(\xi,\tau)}{\partial \xi}\right|_{\xi=1} = 0$, $\theta(s(\tau),\tau) = \theta_c$, with initial conditions $\theta(\xi,0) = \theta_0(\xi)$, $s(0) = s_0$, and phase-change interface dynamics $\frac{ds(\tau)}{d\tau} = -\beta \left.\frac{\partial \theta(\xi,\tau)}{\partial \xi}\right|_{\xi=s^-(\tau)}^{\xi=s^+(\tau)}$, where $\beta := \frac{c_p(T_{\max}-T_{\min})}{\Delta H_c}$. $T_{\min}$ and $T_{\max}$ must be defined such that the non-dimensional temperature remains positive, with $T_{\max}$ being sufficiently large. The non-dimensional variables are then defined as: $\theta(\xi,\tau) :=$

$\frac{T(z,t)-T_{\min}}{T_{\max}-T_{\min}}$, $\tau := \frac{\alpha t}{L^2}$, $\xi := \frac{z}{L}$, $s(\tau) := \frac{s_{\dim}(t)}{L}$ where L is the domain length, $\alpha := k/\rho c_p$ is the molecular thermal diffusivity, k is the thermal conductivity, ρ is the density, and c_p is the isochoric specific heat. Note that we assume that α does not change. In the definition of β, which closely parallels that of a Stefan number, ΔH_c is the enthalpy of denaturation of the tissue. In the above, the phase change (denaturation) occurs at non-dimensional temperature θ_c. Finally, the controlled variable $u(\tau)$, i.e., the non-dimensional heat flux at the boundary, has the following relation with its dimensional counterpart: $u(\tau) = \frac{L}{k(T_{\max}-T_{\min})}\dot{q}''(t)$.

Following material characterization experiments using a Q50 Thermogravimetric Analyzer and a Discovery 2500 Differential Scanning Calorimeter (TA Instruments, Inc.) on porcine loin tissue, we measured the heat capacity in the ambient regime $c_p = 4\,\mathrm{kJ/kg/K}$, latent heat of fusion $\Delta H_c = 250\,\mathrm{kJ/kg}$, and the phase transition temperature $T_c \approx 82\,^\circ\mathrm{C}$. In the following we shall use $T_{\max} = 423.15$ K, $T_{\min} = 273.15$ K, $T_c = 355.15$ K, $\rho = 700\,\mathrm{kg/m^3}$, and $k = 0.5934\,\mathrm{W/kg/K}$. These values were obtained from Valvano et al. (1985), as well as our own experiments on porcine loin tissue.

3.2 Hypermodel Construction

The above-mentioned highly nonlinear two-phase Stefan problem serves as a fundamental basis for expressing the system dynamics in the form amenable to model predictive controller design. To retain the essential system nonlinearities, an appropriate model structure was selected and a dataset for training of the latter was generated.

The dataset was chosen to contain 2000 nondimensional 1-D two-phase Stefan problem solutions of 50 seconds each, sampled with increments of 2.5 seconds. For each sampling period, the PCI location and five temperatures are sampled. The initial conditions are varied randomly, while still maintaining a physically consistent temperature field. The heat flux is constrained to be lower than that generated by a 30 W power setting in direct contact with the domain boundary, and is of bounded time variation (less than one watt per sampling period), with a bias towards maintaining constant power.

We have chosen to express the hypermodel as a discrete-time nonlinear autoregressive system with exogenous input, NLARX (Billings and Wei, 2005). NLARX models can be constructed by training the system on an extensive dataset, while the resulting system is still capable of capturing the inherent nonlinearities in the dynamics observed. We have trained the NLARX model and evaluated it with validation data, with agreement between the phase-change interface locations consistently being over 95% normalized root mean square error.

Heat Distribution Model. While our control input is the electrosurgical probe power, it is necessary to obtain the heat flux at the boundary of each active domain, since this is the control input to the individual 1-D models. To this end, a Gaussian heat input model is used (de Freitas Teixeira et al., 2014; Das et al., 2003): $\dot{q}''(r,P) = \frac{\eta P}{2\pi a}\exp\left(-\frac{1}{4a^2}r^2\right)$, where a is the heat dissipation distance

from the center of the probe (the greater this value, the greater the heat input is spread), r is the distance to the probe tip, P is the probe power, and η is the fraction of the total energy that is conducted by the tissue. We point, however, that an exponential-like decay may also be appropriate depending on the medium features. Such an inspection is outside of the scope of the current work. Following results from de Freitas Teixeira et al. (2014), we are taking $a = 5$ mm, $\eta = 1$. We point out that the results should not be sensitive to variations in the factor a.

Compound Linear Model Construction. To enable the hypermodel to be used in combination with a linear model predictive controller, we must combine several one-dimensional models and linearize the resulting dynamics. For the purposes of generating a local linear model, we consider radius r in the heat distribution model to be equal to the average radius of all active domains, denoted by r_{avg}. By doing so, we effectively approximate the distributed heat flux obtained by the Gaussian heat input model by a single boundary heat flux point source. This is justifiable by considering the sharp decrease in heat flux observed in the heat input model, as well as the fact that the tissue was found to only react to the heat flux in a very small region (< 1 mm) during short periods of time (in the order of 5 seconds).

Determination of the active domains is described in the subsection on the supervisor system. We denote the distances to the probe for each of the N active domains by r_i.

Hypermodel linearization is done by considering an operating point that is equal to the current temperatures at the sampling location, as well as the current PCI location on that domain, as obtained from the maximum temperature field. For domain i, this gives a nondimensional operating point $y_*^{(i)} \in [0,1]^6$. This operating point is converted to the internal linearized model state, which we denote by x_*. Combining this with the present operating power P_*, converted to the nondimensional heat flux u_* at distance r_{avg} from the probe, we then obtain a linearized model $\bar{x}_{k+1}^{(i)} = \bar{A}^{(i)} \bar{x}_k^{(i)} + \bar{B}^{(i)} \bar{u}_k$, $\bar{y}_k^{(i)} = \bar{C}^{(i)} \bar{x}_k^{(i)}$, where the overbar denotes a deviation for the variables (i.e., $\cdot_k = \cdot_* + \bar{\cdot}_k$). Combining the models for the active domains, we can construct the compound linear model as $\bar{A} = \text{diag}\left(\begin{bmatrix} \bar{A}^{(1)} & \cdots & \bar{A}^{(N)} \end{bmatrix}\right)$, $\bar{C} = \text{diag}\left(\begin{bmatrix} \bar{C}^{(1)} & \cdots & \bar{C}^{(N)} \end{bmatrix}\right)$, $\bar{B} = \begin{bmatrix} \bar{B}^{(1)\mathsf{T}} & \cdots & \bar{B}^{(N)\mathsf{T}} \end{bmatrix}^{\mathsf{T}} \dot{q}''(r_{\text{avg}}, 1) \frac{L}{k(T_{\max} - T_{\min})}$.

3.3 Model Predictive Control

In order to obtain our control strategy, it is necessary to solve a model predictive control (MPC) problem that leads to state tracking, while obeying the system's constraints on the minimum and maximum allowable power setting. We use the MPC architecture presented by Diaz Dorado (2018), which incorporates linear constraints.

In our implementation, the MPC solver operates on the compound linear model described previously, with the initial state $\bar{x}_0$ being obtained by considering the deviation between the operating point and the desired operating condition at the present time. The final control inputs are obtained by considering $u_k = u_* + \bar{u}_k$, and converting back to input power P.

Gain matrices. Given that MPC minimizes the cost functional $\sum_{k=0}^{T-1} \left(\bar{u}_k^{\mathsf{T}} R \bar{u}_k + \bar{x}_k^{\mathsf{T}} Q \bar{x}_k \right) + \bar{x}_T^{\mathsf{T}} P \bar{x}_T$, we consider the following structure for the penalty matrices:

$Q = M_Q \times$
$\text{diag}[\exp\left((r_{\min}^2 - r_1^2)/4a^2\right) I, \ldots, \exp\left((r_{\min}^2 - r_N^2)/4a^2\right) I]$,
$P = (M_P/M_Q)Q$, $R = M_R$, where $M_Q, M_P, M_R > 0$, I is an identity matrix of appropriate dimensions, and $r_{\min}$ denotes the distance from the probe to the nearest active heat influx boundary. With this gain structure, we place a higher importance on closer domains.

3.4 Path Planning

Knowing the probe power at a given probe location for a given desired PCI front, we can determine when and how to move the probe along a predesigned path. To enable the latter action, we have created a number of domains of fixed lengths that face perpendicular to the cutting path. For a given probe position, we allow either a step backward, forward, or no movement, with a step size of 5 mm.

To decide the next command of the probe among these three options, we consider both the error at the end of the planning horizon and the initial error for a given probe location. In particular, for each probe position we compute the error: $\epsilon(p_{\text{probe}}) = \bar{x}_T^{\mathsf{T}} P \bar{x}_T + \sum_{i \in \mathcal{A}(p_{\text{probe}})} (s_i - s_d)^{-2}$, where $\mathcal{A}(p_{\text{probe}})$ is the set of admissible domains, defined in the next subsection.

The first term considers the predicted deviation error obtained after applying the MPC-derived control inputs during the entire costing horizon, scaled according to the distance of the probe with respect to the admissible domains. This term incentivizes the system to move in directions where the most progress can be made in satisfying the tracking requirements during the period of the costing horizon, which endows the system with a form of foresight.

The second term serves to disincentivize the system from moving in a direction in which the admissible domains are close to having their tracking goals satisfied. This term drives the system to move to locations where tracking is lacking at the initial time.

Finally, during movement sequences the system maintains the commanded cutting power, with one movement step taking the same amount of time as a sampling period, which is $\Delta t = 2.5$ s. During movement, the system ceases any temperature field updates, to prevent erroneous ones. After a movement step, the local temperature field is embedded into the global temperature field, with its origin offset by the distance moved.

Supervisor system. The set of admissible domains is computed for a given probe location p_{probe}, and depends both on the vicinity to, as well as the PCI location of, each domain. We require the following constraints to be met for a domain i to be considered an admissible domain: $\|p_{\text{probe}} - p_i\| \le r_c$, $|s_i - s_d| \le \Delta s$, where p_i denotes the heat influx boundary of domain i, s_i denotes the PCI location at domain i, s_d is the desired PCI location, and r_c is the

(a) Control command history of the power, and the probe position; $t = 0$ denotes the time of probe engagement.

(b) Final maximum temperature field with domains (green dash-dotted), decision locations (green dots), denaturation front (white solid), and decision temperature front (white dotted).

(c) Photographs of the cut, normal (top), and the same cut spread (bottom), to show the containment of charring (from left to right: trial 1, trial 2).
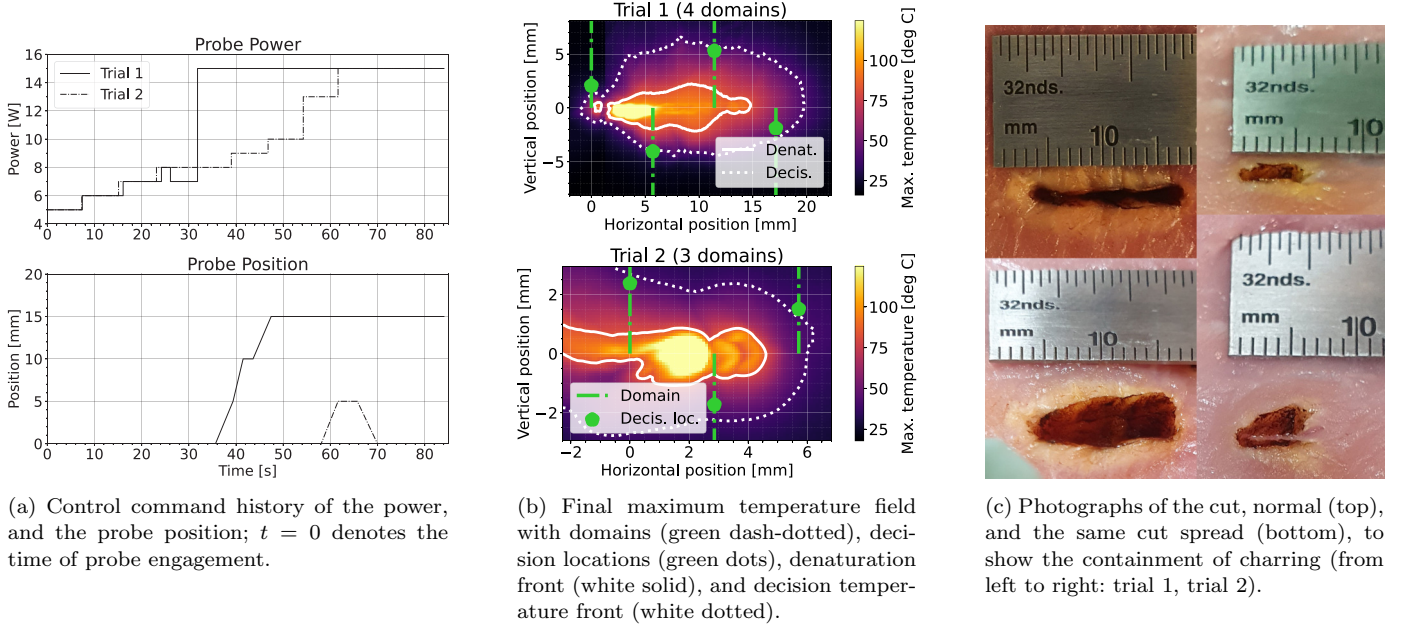
Fig. 4. Basic results of the two line-cutting trials.

cutoff radius. The cutoff radius is taken as 10 mm, since it was observed that the heat input imparts no significant temperature changes beyond this distance. The set of all admissible domains given probe location p_{probe} is denoted by $\mathcal{A}(p_{\text{probe}})$.

At each probe location being considered, the supervisor system instructs the path planning system to skip that location if there are no admissible domains within the cutoff radius. Otherwise, only the admissible domains are considered in the compound model.

Termination of the system is governed by considering $\max_i |s_i - s_d| \leq \Delta s$, $\max_i s_i - s_d \geq \Delta s_{\text{term}}$. If any of these inequalities is satisfied, the system terminates. The first inequality terminates the system based on sufficient tracking of the PCI front, while the latter inequality is based on a maximum allowable overshoot. We take $\Delta s = 0.25\,\text{mm}$, and $\Delta s_{\text{term}} = 0.5\,\text{mm}$, to limit the extent of overshoot.

4. EXPERIMENTS & RESULTS

We performed two line cutting trials on sufficiently large ex vivo porcine loin tissue of approximately flat surface, obtained freshly from the University of Illinois Meat Science Laboratory (Urbana, IL). In trial 1 the goal was to perform a 5 mm deep 15 mm long cut, while limiting the denaturation front to 2.5 mm away from the cutting line. Trial 2 considered a 2.5 mm deep, 5 mm long cut, with a denaturation front of 1 mm. Since errors in the IR thermographer pointing accuracy become more critical as the desired denaturation front location becomes smaller, instead of the location of the bespoke 82 °C denaturation temperature, the tightly related location of the 40 °C isotherm was employed as the decision temperature location, with the desired decision temperature location being twice as far away, i.e., 5 mm, and 2 mm, respectively. Consequently, for feedback, instead of the computed PCI locations, we employ the computed decision

locations obtained by intersecting each domain with the 40 °C isotherm of the maximum temperature field using piecewise linear interpolation. The latter temperature field is the field of aggregated spatiotemporal temperature maxima over a particular trial.

The initial system power was set at 5 W, with the system immediately taking over control after the first solution is obtained. The power was constrained to $P \in [0, 15]$ W. Four 40 mm long domains (Fig. 4b, top image) were considered in trial 1, whereas three domains (Fig. 4b, bottom image) were considered in trial 2. The gain parameters were taken as $M_P = M_Q = 2 \times 10^4$ and $M_R = 0.5$, and were maintained constant to demonstrate transferability of gains across different cutting tasks.

4.1 Control Command History Comparison

In the first trial, we see a relatively slow rise in power up to around 7 W, after which the system ramps up power to the maximum allowable level (15 W); see Fig. 4a. This is due to an increase in the temperature field, but no significant actuation of the decision temperature front, which causes the MPC result to command a saturated control input. In the second trial, a progressive rise pattern is observed, due to the smaller decision front setpoint. Maximum power is also maintained for half the amount of time compared to the first trial. Both system runs terminate at around the same time, after the supervisor system commands termination due to violation of the maximum decision front overshoot margin.

4.2 Maximum Temperature Field Comparison

Fig. 4b illustrates the final maximum temperature fields for both trials. The decision front location is obtained from these plots by considering the isotherm at the decision temperature (white-dotted curve), and intersecting it with the domains. The domains are shown as green dash-dotted lines, with the computed decision location on each domain

denoted by a green dot. Note that the discrepancy between the actual and the computed decision locations is due to image calibration errors accumulated during the system run, and possibly also due to local changes in the index of refraction caused by the inclined view.

For both trials, the supervisor system terminated the system run after one of the domains exceeds the allowable overshoot margin. For trial 1, this was the third domain from the left, whereas for trial 2, this was the first domain from the left.

4.3 Final Cut Topography Comparison

The final cut topography for both trials is shown in Fig. 4c. As expected, the resulting cut length matched the commanded one. For trial 1, the off-white area surrounding the cut has a front distance of approximately 2.5 mm, and matches the denaturation temperature field footprint. This holds less so at the two extremes, with some discrepancy being observed at the leftmost boundary.

For the second trial, disregarding the high-temperature streak on the left, the temperature-derived denaturation front closely matches the off-white area surrounding the cut. Once again, the cut has a denaturation area that extends about 1 mm transversely from the cutting line. Both results support approximation of the denaturation front by a maximum ($82\,^{\circ}$C) temperature isotherm.

5. DISCUSSION

The probe movement during the cut gives rise to small unaccounted for pointing errors, resulting in thermographer misalignment and preventing the system from performing longer and more complex cuts. Therefore, an improvement in thermographer pointing precision is currently being pursued through hardware refinement.

In the $82\,^{\circ}$C isotherm marked on the maximum temperature field of trial 2 shown in Fig. 4b, a high-temperature streak can be seen to extend due left. The latter depicts not the surface temperature, but rather a high-temperature particle stream that is traveling towards the suction system. Redesigning the latter to minimize this streak will be addressed in future work.

Saturation-like power level behavior towards the end of a run represents a feedback-based satisfaction of the denatured boundary layer width constraint. A slow rise in power allows slow PCI movement, permitting the system to avoid denatured tissue width overshoot. However, the desired denatured layer width limits the cutting depth in the current control law. Minimizing tissue damage while providing the desired cutting depth through feedback-controlled power manipulation is the subject of future work.

6. CONCLUSION

We described control-oriented process model development, path planning, and tissue experimentation on an autonomous electrosurgery platform. The system is the first to place an explicit focus on performing cutting tasks while controlling the denaturation front, relying solely on temperature feedback. We showed a platform with collocated sensing and actuation capabilities, and outlined procedures for tuning the system parameters. The system satisfactorily tracked a given desired denaturation front, while accurately completing cutting tasks. The ability to perform cutting tasks without imparting excessive heat damage onto the surrounding tissue demonstrates the feasibility of autonomous electrosurgical systems for regular and infracentimetric cutting tasks.

REFERENCES

Beasley, R.A. (2012). Medical Robots: Current Systems and Research Directions. *Journal of Robotics*, 2012, 1–14. doi:10.1155/2012/401613.

Billings, S. and Wei, H.L. (2005). A New Class of Wavelet Networks for Nonlinear System Identification. *IEEE Transactions on Neural Networks*, 16(4), 862–874. doi:10.1109/TNN.2005.849842.

Cannon, J.R. (1984). *The One-Dimensional Heat Equation*. Number v. 23 in Encyclopedia of Mathematics and Its Applications. Addison-Wesley Pub. Co, Reading, Massachusetts.

Das, S., Klotz, M., and Klocke, F. (2003). EDM simulation: Finite element-based calculation of deformation, microstructure and residual stresses. *Journal of Materials Processing Technology*, 142(2), 434–451. doi:10.1016/S0924-0136(03)00624-1.

de Freitas Teixeira, P.R., de Araújo, D.B., and da Cunda, L.A.B. (2014). Study of the Gaussian distribution heat source model applied to numerical thermal simulations of TIG welding processes. *Ciência & Engenharia (Science & Engineering Journal)*, 23(1), 115–122.

Diaz Dorado, A. (2018). *Efficient Convex Quadratic Optimization Solver for Embedded MPC Applications*. Master's Thesis, KTH, School of Electrical Engineering and Computer Science, Stockholm, Sweden.

El-Kebir, H. and Bentsman, J. (2021). PDE-Based Modeling and Non-collocated Feedback Control of Electrosurgical-Probe/Tissue Interaction. In *2021 American Control Conference*. IEEE, New Orleans, Louisiana, USA.

Opfermann, J.D., Leonard, S., Decker, R.S., Uebele, N.A., Bayne, C.E., Joshi, A.S., and Krieger, A. (2017). Semi-autonomous electrosurgery for tumor resection using a multi-degree of freedom electrosurgical tool and visual servoing. In *2017 IEEE/RSJ International Conference on Intelligent Robots and Systems (IROS)*, 3653–3660. IEEE, Vancouver, BC. doi:10.1109/IROS.2017.8206210.

Palanker, D., Vankov, A., and Jayaraman, P. (2008). On mechanisms of interaction in electrosurgery. *New Journal of Physics*, 10(12), 123022. doi:10.1088/1367-2630/10/12/123022.

Saeidi, H., Ge, J., Kam, M., Opfermann, J.D., Leonard, S., Joshi, A.S., and Krieger, A. (2019). Supervised Autonomous Electrosurgery via Biocompatible Near-Infrared Tissue Tracking Techniques. *IEEE Transactions on Medical Robotics and Bionics*, 1(4), 228–236. doi:10.1109/TMRB.2019.2949870.

Valvano, J.W., Cochran, J.R., and Diller, K.R. (1985). Thermal conductivity and diffusivity of biomaterials measured with self-heated thermistors. *International Journal of Thermophysics*, 6(3), 301–311. doi:10.1007/BF00522151.